

Identification of sub-angstrom many-body localization in quantum materials by Bragg scattering phase breaking and ultrafast structural dynamics

Yingpeng Qi^{1,2#*}, Jianmin Yang^{3,4#}, Zihui Zhou², Qing Xu², Yang Lv², Xiao Zou², Tao Jiang², Pengfei Zhu², Dongxue Chen^{1,5}, Zhenrong Sun⁶, Lin Xie^{7*}, Dao Xiang^{2,8*}, Jiaqing He^{3,9*}

¹Suzhou Institute for Advanced Research, University of Science and Technology of China, Suzhou 215123, China

²Key Laboratory for Laser Plasmas (Ministry of Education), School of Physics and Astronomy, Shanghai Jiao Tong University, Shanghai 200240, China.

³Department of Physics, State Key Laboratory of Quantum Functional Materials, and Guangdong Basic Research Center of Excellence for Quantum Science, Southern University of Science and Technology, Shenzhen 518055, China.

⁴Department of Materials Science and Engineering, National University of Singapore, 117575, Singapore.

⁵Department of Physics, University of Science and Technology of China, Hefei, Anhui 230026, China

⁶State Key Laboratory of Precision Spectroscopy, and School of Physics and Electronic Science, East China Normal University, Shanghai 200241, China

⁷School of Physical Sciences, Great Bay University, Dongguan 523000, China.

⁸Zhangjiang Institute for Advanced Study, Shanghai Jiao Tong University, Shanghai 201210, China.

⁹Guangdong Provincial Key Laboratory of Advanced Thermoelectric Materials and Device Physics, Southern University of Science and Technology, Shenzhen, 518055, China

#Contributed equally

*Correspondence to qypcool@ustc.edu.cn, xielin@gbu.edu.cn, dxiang@sjtu.edu.cn, hejq@sustech.edu.cn.

Defects, fluctuations, degenerate states and correlated interactions facilitate the emergence of exotic properties in condensed matter systems while also inducing atomic-scale local correlated structures that deviate from the average long-range order. Establishing the structure-property relationship from the perspective of these atomic-

scale local correlated structures-rather than relying on phenomenological description of the electron, phonon, spin and orbital freedoms based on mean-field theory-remains ambiguous and controversial due to the lack of direct methods for identifying such local correlated structures. In this work, based on the photoexcited ultrafast structural response, we propose a Bragg scattering phase breaking regime to identify the sub-angstrom local correlated structures in quantum materials. With this regime, we unambiguously identify the many-body-interaction driven local correlated structures with static off-center Ag displacements of $0 \sim 0.5 \text{ \AA}$ in the low temperature ground state of AgCrSe₂. As temperature rising, these static local correlated structures transform to a dynamic state where the thermal fluctuations overwhelm the multiple localized quantum states, signifying the strong anharmonicity of the local structures. The state-of-the-art density functional theory simulation well reproduces the intrinsic many-body-interaction driven local correlated structures. These unique local correlated structures evidence the first many-body localization with topological order characteristic in real material systems and provide a unified scenario for the versatile quantum properties in single crystalline AgCrSe₂. Our work not only offers a universal approach to characterize sub-angstrom local correlated structures across a wide range of quantum materials but also deepens our understanding of the fundamental mechanism behind exotic properties from the perspective of atomic-scale local correlated structures.

The structure of materials fundamentally determines their properties, which is a traditional paradigm across various fields in condensed matter physics and materials science [1-4]. Resolving the structure-property relationship is therefore pervasive throughout the research field [5-7], spanning crystalline to amorphous material systems. For crystalline materials, symmetry analysis based on ideal/average crystal structure and mean-field approximation has been well-established for quantifying material properties both experimentally and theoretically [3,8-10]. However, defects, fluctuations, degenerate states and correlated interactions introduce complexity into the crystal structure, leading to atomic-scale local correlated structures that deviate from the long-range average structure [11-25]. These local correlated structures, with correlation lengths limited to sub-unit cell to a few unit cells, underpin many exotic properties incompatible with average symmetry and mean-field theory. Examples include topological order [7,26], high temperature superconductivity [27], anomalous Hall effect [22], relaxor ferroelectrics [28,29], quantum light emission [30,31] and strange metals [25,32], which mainly drive by either extrinsic defects or intrinsic many-body interactions. Note that, the interplay of interactions and disorder in a quantum many body system may lead to the phenomenon of many body localization (i.e., the topological order [7,26]) with the breakdown of thermodynamics [33,34], which has yet to be identified in real material systems. Significant efforts have been devoted to characterize these atomic-scale local structures and bridge the relationship between the local structures and exotic properties through experimental and theoretical approaches [5,35,36], such as Raman and X-ray fine absorption spectrum [12,37],

scanning transmission electron microscopy enhanced by computational techniques [38,39], X-ray and neutron diffraction [36,40] and computational predictions enhanced by machine learning models [5,41,42]. The lack of the statistic feature of the local probe [38,39] and the difficulty of retrieve local structure from halo-like diffuse scattering [36,40] urge novel methods with sub-angstrom spatial resolution. Moreover, all present approaches acquire the information of the local structures at equilibrium states; neither the dynamical response of the local structures nor the identification of the local structure with dynamical response has been achieved. As a result, elucidating the structure-property relationship from the perspective of atomic-scale local correlated structures remains an appealing yet unattained goal.

In this work, we establish a systematic methodological framework that employs ultrafast structural response via femtosecond electron diffraction to identify atomic-scale local correlated structures. Fig. 1A manifests the schematic representation of the femtosecond electron diffraction system. The femtosecond laser pulse serves as the external stimulation, and at varying time delays, the femtosecond electron pulse probes the diffraction pattern change, thereby extracting vibrational and displacive responses of the materials. The intensity of the Bragg reflection is proportional to the square of the structure factor: $I_{hkl} \propto |F_{hkl}|^2$. The structure factor of the Bragg reflection (hkl) at the time delay t is expressed as follows:

$$F(hkl, t) = \sum_j T_j(t) \cdot F_j(t) = \sum_j T_j(t) \cdot f_j \cdot \exp\left(-i \cdot 2\pi \cdot s_{hkl} \cdot (r_j + \mu_j + \kappa_j(t))\right) \quad (1)$$

$$T_j(t) = \exp(-8\pi^2 \langle v_j(t)^2 \rangle s_{hkl}^2) \quad (2)$$

where the summation runs over all atoms within the local structures, f_j denotes the atomic form factor for the j th atom, T_j represents the thermal vibrations, s_{hkl} is the scattering vector, r_j indicates the vector position of the j th atom, μ_j is the intrinsic static local displacement induced by local correlated structure, $\kappa_j(t)$ signifies the photoinduced displacement and v_j denotes the amplitude of the thermal vibration. For each atom, the structure factor F_j is a complex number, composed of $F_{j,\text{real}}$, $F_{j,\text{imag}}$ and the phase angle θ_j . In an ideal/average crystal structure with $\mu_j = 0$, some special characteristic Bragg peaks (hkl) exhibit the property that the phase (and the imaginary part of the structural factor) for each atom is zero, i.e. $\theta_j = 0$. This unique phase characteristic causes the intensity changes of these peaks to follow an s^2 dependence ($|F|^2 \propto s^2$, $\ln(|F|^2) \propto s^2$) as the amplitude of thermal vibrations increases within a relatively small range and/or photoinduced displacement $\kappa_j(t)$ with relatively small amplitude gets involved. This small amplitude approximation for vibrations and displacements is generally effective because even reaching the Lindemann's melting criterion, the square root of the particle mean-squared displacement from the equilibrium position is just ~ 0.1 of the interparticle distance. However, in real crystal structures, local atomic displacements ($\mu_j \neq 0$) are probably introduced in the ground state induced by defects, fluctuations, degenerate states and correlated interactions. In this case, the phase and the imaginary part become nonzero, i.e. $\theta_j \neq 0$, giving rise to the Bragg scattering phase breaking regime and the anomalous intensity changes disrupting the s^2 dependence. This is termed the Bragg scattering phase breaking regime, a manifestation of the geometric phase [43], as illustrated in Fig. 1B. Therefore, the

disrupting of the s^2 dependence serves as a signature of local structures deviating from the average symmetry and reversely, the local correlated structures can be extracted from the anomalous intensity changes across the characteristic Bragg peaks. The transverse coherence length of femtosecond electron pulse is a few nanometers, so it is sensitive to the local displacement ranging from sub-unit cell to a few unit cells. Note that, both vibrational response and displacive response by external stimulation contribute to the anomalous intensity changes across the characteristic Bragg peaks. With femtosecond electron diffraction, the temporal separation of these two intertwined physical processes-namely, the much faster displacive response compared to the vibrational response [44,45], enables the precise quantification of local structures. Other probable physical response, such as the relaxation of local strain [46], can also be identified by ultrafast structural dynamics and used to construct the local correlated structures. Any measurement at equilibrium state will suffer complexity and entanglement of these physical responses and obstacle quantifying local correlated structures. Therefore, the Bragg scattering phase breaking regime together with femtosecond electron diffraction compose a systematic methodological framework to identify atomic-scale local correlated structures and construct the structure-property relationship in quantum materials.

In this study, we take the single-crystalline quantum material AgCrSe_2 as a model system to verify this novel methodology because the versatile anomalous properties in this material system hint at atomic-scale local correlated structures. The phonon spectrum AgCrSe_2 by many-body perturbation theory displays significant low-

frequency phononic flat bands (~ 0.7 THz) [47]. Analogous to electronic flat bands resulting from strong correlation and localization [48], these phononic flat bands have been theoretically predicted to host extreme localizations in the lattice freedom [29], however, the direct structure evidence is absent. At low temperature (~ 9 K), AgCrSe₂ displays an anomalous boson-peak-like feature [49] indicating excessive vibrational modes in the THz range, while the boson peak is of unique many-body driven characteristic of amorphous materials [50,51]. Such a boson-peak-like feature is expected to contribute to the ultralow thermal conductivity of AgCrSe₂ [49], yet the structural origin is not clear. Note that, even in amorphous materials, the origin of boson peak from either disordered atomic packing or random fluctuation of force constants remains a controversy [51,52]. With inelastic neutron scattering, the vibrational spectrum of AgCrSe₂ display unexpected vibration peaks spanning ~ 0.5 - 4.5 meV at low temperature (10-40 K) and the peaks around 0.5-2 meV disappear at the temperature above 300 K [53], indicating strong local anharmonicity [54]. The structural origin of this local anharmonicity has yet to be identified. AgCrSe₂ also has rich magnetic properties, such as the spiral spin liquid state [55] and the anomalous Hall effect [56], and these exotic magnetic behaviors always suffer complexity from the local crystal structure [22,57]. In the spiral spin liquid state at below 30 K, the origin of the extensive degenerate ground states and the associated strong short-range correlations remain unclear [55,58]. For the anomalous Hall effect (AHE) in AgCrSe₂, the time-reversal symmetry breaking in the low-temperature antiferromagnetic phase remains to be understood, moreover, the identification of the mechanism of AHE, either

intrinsic (Berry-phase curvatures) or extrinsic (disorder scattering), has been a long standing question due to the limitation in resolving the structural disorder in real materials [22,56]. Ideally, AgCrSe_2 hosts a hexagonal crystal structure with alternative Ag layers and CrSe_6 octahedral layers repeating along the c axis [59], as shown in Fig. 1C. At T_c of about 450 K, the space group of crystal symmetry changes from $R3m$ to $R-3m$. Both the two phases hold characteristic Bragg reflections (110), (220) and (330) with the imaginary part of the structural factor to be zero. In this work, with femtosecond electron diffraction and the novel Bragg scattering phase breaking regime, we reveal static correlated Ag displacements deviating from the ideal sites in single-crystalline AgCrSe_2 , as illustrated in Fig. 1C. As temperature rising, these static local correlated structures transform to a dynamic state where the thermal fluctuations overwhelm the multiple localized quantum states. These unique local correlated structures evidence the first many-body localization with topological order characteristic in real material systems and provide a unified scenario for the versatile quantum properties in single crystalline AgCrSe_2 , such as the phononic flat bands, the Boson-peak-like anomaly, the extreme local anharmonicity, the electronic flat bands, the spiral spin liquid and the anomalous Hall effect.

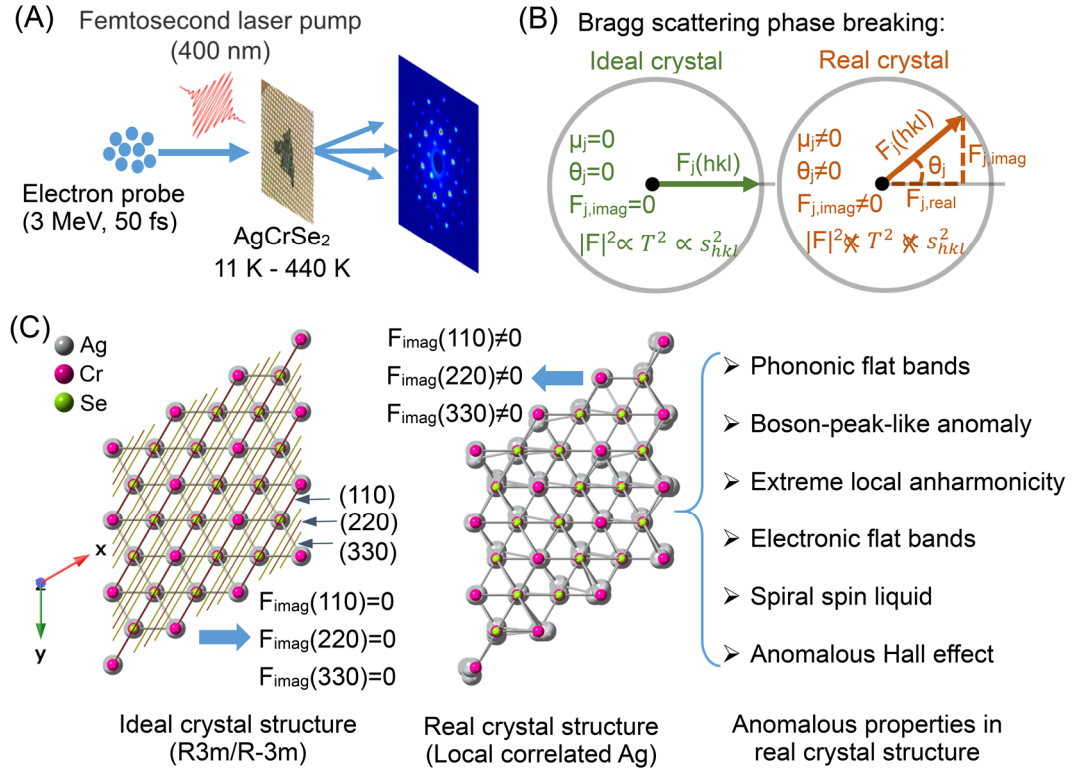


Fig. 1 (A) Schematic representation of the femtosecond electron diffraction system. (B) Schematic illustration of the identification of local correlated structures with Bragg scattering phase breaking regime. The complex form of the structure factor $F(hkl)$ illustrated by a circular diagram. The amplitude F_{real} is represented as the radius of the circle and the phase F_{imag} as the angle made to the horizontal direction. The local displacement μ_j makes Bragg scattering phase $\theta_j \neq 0$, disrupting the s^2 dependence of the Bragg intensities. (C) Contrast between the ideal crystal structure and the real crystal structure of AgCrSe₂. The anomalous properties associated with the local correlated Ag is displayed in the right.

The single crystalline AgCrSe₂ sample with the thickness of ~ 50 nm is prepared and transferred onto a TEM copper grid for subsequent experiments (see sample

preparation in Supplementary Materials). Fig. 1A displays the schematic representation of the femtosecond electron diffraction setup (see details in Supplementary Materials). The sample is pumped with 400 nm femtosecond laser at the base temperature of 11-440 K. The ~ 50 fs temporal resolution of our femtosecond electron diffraction system [60] allows for the detection of the fastest structural response in most material systems, thereby fulfilling the experimental requirement efficiently. The differential diffraction pattern at the time delay of ~ 6 ps and the time-resolved structural response of the several characteristic Bragg peaks at 100 K are shown in Fig. 2A and 2B, respectively. The monotonic intensity decay from femtosecond to picosecond timescales indicates enhanced thermal vibrations. Therefore, the intensity changes across these peaks are expected to follow a linear q^2 dependence under small perturbation. However, the experimental intensity change $-\ln(I/I_0)$ at the time delay of ~ 6 ps, as shown in Fig. 2C, deviates significantly from the linear dependence. For example, the intensity change of (220) is expected to four times larger than that of the (110), while in experimental results, the intensity of (110) decays by $\sim 5\%$ and the (220) show somewhat intensity enhancement. Such anomalous intensity changes arise since the onset of the structural response and persists as varying pump fluence, indicating that it is an intrinsic property of the material. The six reflections of the $\{220\}$ crystal plane family labeled by green circles display the same anomalous intensity change, so the possible impact from sample tilting and crystalline domain can be neglected. At the much lower temperature of 11 K, the similar structural response deviating from linear dependence is shown in Fig. S1 in Supplementary Materials. Possible contributions from multiple scattering,

photoinduced displacements and local strains are excluded (see Supplementary Materials). All above analyses point to static atomic-scale local structures in AgCrSe₂ at low temperatures, which break the zero phase of these characteristic Bragg peaks and give rise to anomalous intensity changes. In contrast, the structural response at the elevated temperature of 440 K follows a quasi-linear q^2 dependence, as shown in Fig. 2D-2F. For instance, the intensity change of (220) is as expected to around four times larger than that of the (110). The high temperature of 440 K is close to the transition temperature of the R-3m phase. Both the low temperature R3m phase and high temperature R-3m phase exhibit zero phase for these characteristic Bragg peaks, so the linear q^2 dependence is expected for both phases. The structural transition from R3m to R-3m mainly derives from the interlayer Ag displacements and the host sublattice CrSe₂ remains stable across temperatures [59]. Therefore, we attribute the atomic-scale local structures at low temperature to local Ag displacements deviating from the ideal sites in the ideal/average crystal structure. The multiple local correlated Ag displacements compose the average Ag position in the ideal R3m phase. As the temperature rising, the thermal fluctuation suppresses and overwhelms the local Ag displacement and then gives rise to the linear q^2 dependence as expected, so a static to dynamic transition of the local structures unifies the complete physical process.

We take the ratio between the intensity change of I_{220} and I_{110} , i.e. $\Delta I_{220}/\Delta I_{110}$, as the parameter to evaluate the static to dynamic transition of the local structure, as shown in Fig. 3A. As temperature rising, the ratio gradually changes from the negative values to the theoretically predicted value of ~ 4 with the ideal crystalline structure,

unambiguously evidencing the temperature-driven static to dynamic transition of the local structures. At the fixed temperature of 330 K, we observe the ratio gradually changes from ~ 2 to the expected value of ~ 4 as increasing the pump fluence, therefore, the laser pump also modulates the local structures. Such a continuous transition with multiple intermediate states featured with local correlated structures is beyond the conventional framework of first/second order transition and the Landau transition theory [3,9]. Fig. 3B illustrates the physical scenario revealed in our study: a transition from the static local structures below 100 K to the dynamic local structures at 440 K. In the real material system of AgCrSe_2 , at the temperature below 100 K, multiple local potential minima (e.g., p_0 , p_1 , p_2 in Fig. 3B) instead of a single minimum allow Ag atoms at different crystal sites to occupy positions deviating from their ideal positions. These static Ag site deviations induce local vibrations and potentially excess vibrational density of states. At the high temperature above 440 K, the thermal fluctuation overwhelms the potential barriers among multiple local minima. As a result, the dynamic Ag deviations with random occupation of multiple local minima emerge, giving rise to the averaged occupation of the ideal crystal sites. In the range of 100 K \sim 440 K, the competition between the local correlated interaction and the thermal fluctuation leads to multiple intermediate states.

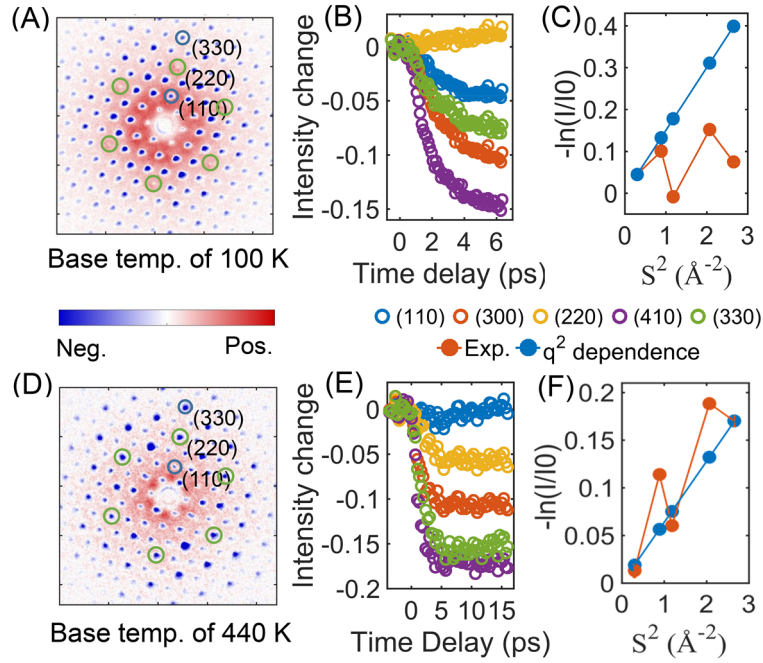


Fig. 2 Experimental results with the base temperature of 100 K (A-C) and 440 K (D-F) and the pump fluence of 3.4 mJ/cm^2 . (A) Differential diffraction pattern at the time delay of $\sim 6 \text{ ps}$. The circles label the characteristic Bragg peaks (110), (220) and (330). (B) Experimental intensity changes of characteristic Bragg peaks at 100 K. (C) The s^2 (i.e., q^2) dependences of the experimental results at 100 K and the theoretical prediction results. (D) Differential diffraction pattern at the time delay of $\sim 6 \text{ ps}$. (E) Experimental intensity changes of characteristic Bragg peaks at 440 K; (F) The s^2 (i.e., q^2) dependences of the experimental results at 440 K and the theoretical prediction results.

To quantify the atomic-scale local structures, we perform structure factor calculations by incorporating local Ag displacements to reproduce the experimental anomalous intensity changes observed at the low temperature. To simplify the calculation, we use a single unit cell, rather than a supercell, to model the diffraction intensity change of the overall lattice. Nine parameters are utilized to constrain the local

structure model with the formula (1) in the previous section: the displacements along the x and y axes for the three Ag atoms in the unit cell, as well as the three vibrational amplitudes for Ag, Cr and Se atoms respectively (see calculation details in Supplementary Materials). 48 local structures and their corresponding vibration amplitudes are identified as shown in Table S3 in Supplementary Materials. Fig. 3C displays the contrast between the unit cell in the ideal R3m phase and the identified local structure with local Ag displacements (i.e., the first structure listed in Table S3 in Supplementary Materials). The local Ag displacement as large as 0.37 Å is widely observed across these local structures. To simulate the time-resolved intensity change, the thermal vibrations gradually increase to the identified value with the same time constant as that of the experimental results. With the local structure shown in Fig. 3C (bottom), the simulated intensity changes of the characteristic Bragg peaks as a function of the time delay manifest in Fig. 3C (top). These simulation results well reproduce the experimental results in Fig. 2B. Therefore, the structure factor calculation quantitatively identifies the static local structures with local Ag displacements in single-crystalline AgCrSe₂. As we expand the boundary of the amplitude of the Ag displacements to ~ 0.5 Å, more than a thousand local configurations enable to reproduce the experimental results. The finite number of the local configurations indicates that the local displacements among Ag atoms are correlated and non-ergodic instead of random. The present calculation is based on a single unit cell, so the identified local structures represent an average of the local structures in real materials. A more precise structural model with a supercell is expected and demands much computational source, which is beyond the

scope of the present work.

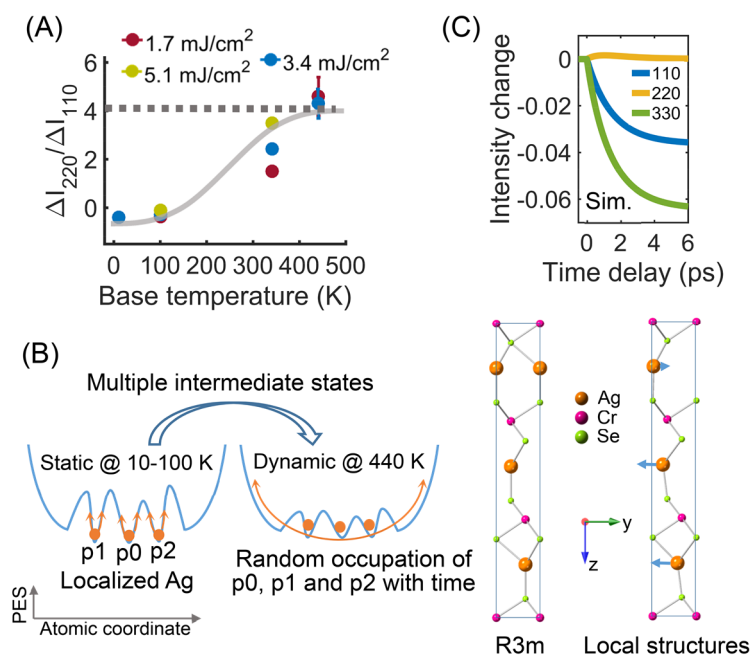


Fig. 3 (A) $\Delta I_{220}/\Delta I_{110}$ as a function of the base temperature and pump fluence. The solid line is a guide to the eye and the dotted line is the theoretically predicted ratio from the ideal crystalline structure. (B) Schematic representation of the static to dynamic transition of the local structures from the perspective of potential energy landscape. (C) (top) Simulated intensity change as a function of time with local correlated structures. (bottom) Rigid unit cell in the R3m phase (left) and the local correlated structure with Ag displacements indicated by arrows (right).

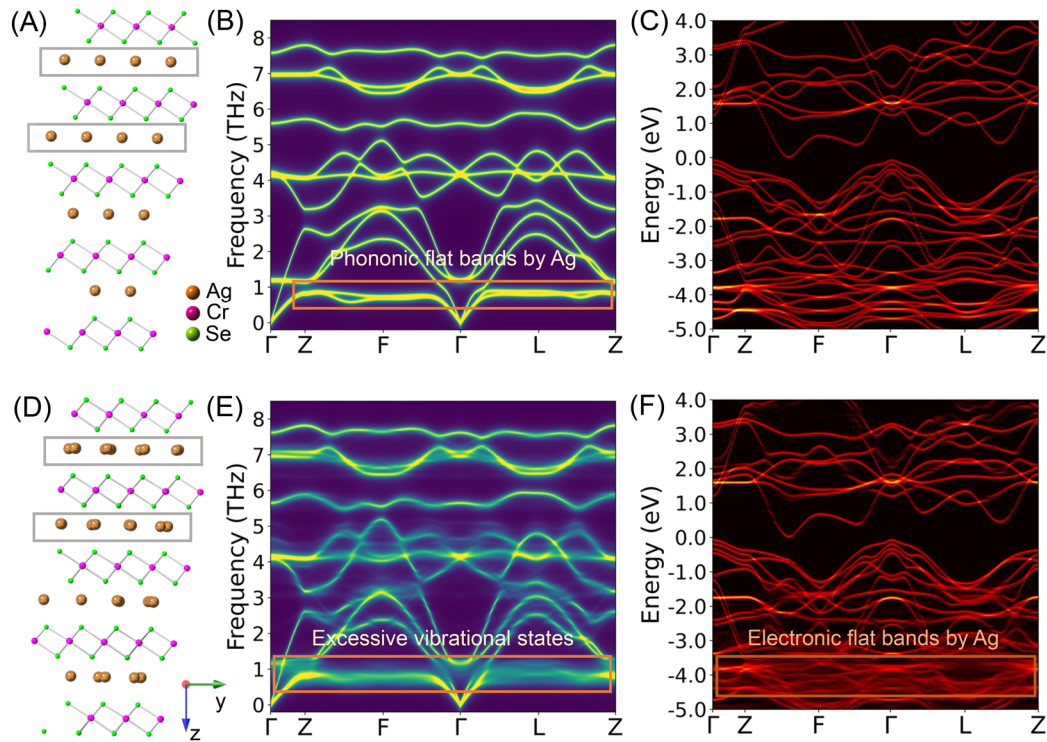


Fig. 4 DFT simulation of the ideal high-symmetry R3m structure (A-C) and the real R3m structure with local correlated Ag displacements (D-F). (A) Ideal R3m crystal structure with rigid Ag positions at the center of the Se tetrahedra. (B) Phonon spectral function along the high symmetry lines. The spectrum in the rectangle indicates the phononic flat bands dominated by Ag. (C) Electron band structure along the high symmetry lines. (D) Real crystal structure with local correlated Ag displacements. (E) Phonon spectral function along the high symmetry lines. The spectrum in the rectangle indicates the excessive vibrational states induced by local Ag displacements. (F) Unfolded electron band structure along the high symmetry lines. The spectrum in the rectangle indicates the electronic quasi-flat band induced by local Ag displacements.

To further quantify the local correlated structures in the low temperature phase of AgCrSe_2 , we perform Density-functional theory (DFT) simulations. In the framework of density-functional perturbation theory, the supercell with 256 atoms is stable in the ideal $R3m$ phase and the Ag atoms uniformly located at high symmetry positions, as shown in Fig. 4A. The phonon spectral function in Fig. 4B manifests remarkable phononic flat band at around 0.7 THz and the Ag atoms dominate these low-frequency flat bands. The electron band structure of the ideal $R3m$ phase is shown in Fig. 4C and the Ag atoms dominate the deep level electronic band around -4 eV. By applying anharmonic special displacements to the supercell and then allowing a full relaxation of all the ion positions (see details in Supplementary Materials), the relaxed supercell in Fig. 4D displays remarkable local Ag displacements deviating from the ideal sites, meanwhile, the positions of Cr and Se atoms remain unchanged. The energy for the supercell with local correlated structures is lower than that of the ideal structure by ~ 1 meV/atom, therefore, these local structures are energetically favorable. Most Ag atoms host significant local displacements and the maximum amplitude is ~ 0.5 Å, which is comparable to the value of 0.37 Å by structure factor calculation in Fig. 3C. In Fig. 4E, the phonon spectral function of the supercell with local structures do not show any signature of imaginary frequency, indicating that the supercell is dynamically stable. Excessive vibration states emerge at around 0.7 THz frequency and higher frequencies (~ 1 THz along Γ -Z) due to the local displacements of Ag atoms. In the electron spectral function in Fig. 4F, excessive band structures emerge at around -4 eV and give rise to a quasi-flat band feature. The Ag atoms dominate these deep-level electronic band

structures, so the quasi-flat band feature is closely associated with the anomalous local structures. Analogous to electronic flat bands resulting from strong correlation and localization [48], phononic flat bands have been theoretically predicted to host extreme localizations in the lattice freedom [29]. To the best of our knowledge, the localized Ag displacement featured with phononic flat bands is the first experimental exemplification of the many-body localization in real material systems. As a sister compound of AgCrSe_2 , CuCrSe_2 shows no signature of phononic flat bands in its phonon spectrum [53]. In our femtosecond electron diffraction for CuCrSe_2 , the intensity change of the characteristic Bragg peaks at 100 K follows a very linear s^2 dependence, suggesting no Cu local displacements. Therefore, the local Ag displacements and the phononic flat bands are directly and deterministically linked.

In this study, with the combination of the femtosecond electron diffraction, the novel Bragg scattering phase breaking regime, the sophisticated structure factor calculation and the state-of-the-art density functional theory simulation, we unambiguously reveal the many-body driven sub-angstrom local correlated Ag displacements in the quantum material AgCrSe_2 . The competition between the many-body localization and the thermalization gives rise to a localization-delocalization transition (i.e., a static to dynamic transition) of the local correlated structures as temperature rising from 11 K to 440 K. The phononic flat bands, the local Ag displacements by simulation and experiment and the thermalization as temperature rising compose a complete physical image of the many body localization and the topological order in the lattice freedom. The local Ag displacements at low temperature

produce excessive vibrational modes at the low frequency of ~ 0.7 THz (~ 3 meV) as shown in Fig. 4E. The inelastic neutron scattering clearly displays extra vibration peaks at around 0.5-2 meV at low temperature (10-40 K) [53]. These vibration features exclusively confirm the local Ag displacements as the structural origin of the anomalous boson peak [49] in the crystalline AgCrSe₂. Note that, these extra vibration peaks by many-body localization probably represent kind of fractional excitations in the lattice freedom, analogous to the fractional electronic excitation [61,62]. As the temperature goes above 300 K, the vibration peaks around 0.5-2 meV disappear in the inelastic neutron scattering [53], meanwhile, the local Ag displacement is significantly suppressed in our experiment. Therefore, the extreme anharmonicity in the vibration spectrum derives from the local correlated structures, which is expected to be a universal mechanism dominating extreme anharmonicity in material systems [54]. The recent study demonstrates the indirect superexchange interactions through Cr-Se-Ag-Se-Cr path between the adjacent CrSe₆ octahedral layers [63]. By superexchange interactions, the multiple local correlated structures indicated by Ag displacements probably break the interlayer antiferromagnetic state and induce the spiral spin liquid state featured by extensive degenerate ground states and strong short-range correlations [55,58]. Moreover, these local correlated structures constitute a structural origin of the time-reversal symmetry breaking for the anomalous Hall effect (AHE) in AgCrSe₂ [22,56]. The identification of the mechanism of AHE, either intrinsic (Berry-phase curvatures) or extrinsic (disorder scattering), has been a long standing question due to the limitation in resolving the structural disorder in real materials. Our work provide a

solution towards resolving this question.

Pursuing atomic-scale local structure characterization is actually entering a realm where the idea of constructing a three dimensional crystal with a unit cell is only partly valid [64]. Alternatively, the average over a multitude of local structures constructs what is called the average crystal structure. In this study, we propose the Bragg scattering phase breaking regime to unambiguously reveal the sub-angstrom local structures deviating from the average crystal structure in crystalline materials. This novel regime has an intrinsic advantage in distinguishing the static displacements from dynamic vibrations, which is significant in constructing structure-property relationship but fails in other probing techniques. Instead of photoinduced structural dynamics [65,66], we extend the femtosecond electron diffraction to study the intrinsic anomalous structural characteristic in the ground state in quantum materials. Plenty materials exhibit characteristic Bragg peaks as summarized in Supplementary Materials, so the Bragg scattering phase breaking regime, combined with femtosecond electron diffraction, provides a powerful approach for uncovering hidden local structures and bridging the structure-property relationship from the perspective of atomic-scale local structures in condensed matter physics and material science.

Acknowledgements

Funding: This work was supported by National Natural Science Foundation of China (12304024, 12574045, 12525501, 12335010) and National Key R&D Program of China (no. 2024YFA1612204). D.C. acknowledges the support from National

Natural Science Foundation of China (Grant Numbers 12574348) and Natural Science Foundation of Anhui Province (Grant Numbers 2408085MF176). D. X. would like to acknowledge the support from the New Cornerstone Science Foundation through the Xplorer Prize. The UED experiment was supported by the Shanghai soft x-ray free electron laser facility. J. H. acknowledges the support from the National Key Research and Development Program of China (2024YFB3813800), the National Natural Science Foundation of China (Grant No. 12434001, 52461160258, U25A20239), Guangdong Provincial Key Laboratory of Advanced Thermoelectric Materials and Device Physics (Grant No. 2024B1212010001), the Outstanding Talents Training Fund in Shenzhen (Grant No. 202108) and 2024JC08A027. Author Contributions: Yingpeng Qi devised the project and conceived the presented ideas. Jianmin Yang prepared and characterized the sample. Yingpeng Qi performed the MeV femtosecond electron diffraction experiments with help from Zhihui Zhou, Qing Xu, Yang Lv, Xiao Zou, Tao Jiang and Pengfei Zhu. Yingpeng Qi analyzed the experimental data and built up the model presented in the paper. Lin Xie performed the DFT simulation. Yingpeng Qi wrote the paper with contributions from all other authors. Yingpeng Qi, Lin Xie, Dongxue Chen, Zhenrong Sun, Dao Xiang and Jiaqing He supervised the project. Competing interests: The authors declare no competing interest. Data and materials availability: All data needed to evaluate the conclusions in the paper are present in the paper and/or the Supplementary Materials. Additional data related to this paper may be requested from the corresponding author Yingpeng Qi.

1. P. W. Anderson, *More Is Different - Broken Symmetry and Nature of Hierarchical Structure of Science*, *Science* 177, 393 (1972).
2. T. Senthil, *Symmetry-Protected Topological Phases of Quantum Matter*, *Annual Review of Condensed Matter Physics*, Vol 6 6, 299 (2015).
3. P. C. Hohenberg and A. P. Krehov, *An introduction to the Ginzburg-Landau theory of phase transitions and nonequilibrium patterns*, *Physics Reports-Review Section of Physics Letters* 572, 1 (2015).
4. A. Simonov and A. L. Goodwin, *Designing disorder into crystalline materials*, *Nature Reviews Chemistry* 4, 657 (2020).
5. I. Mosquera-Lois, S. R. Kavanagh, J. Klarbring, K. Tolborg, and A. Walsh, *Imperfections are not 0 K: free energy of point defects in crystals*, *Chem Soc Rev* 52, 5812 (2023).
6. D. Sarkar, A. Bhui, I. Maria, M. Dutta, and K. Biswas, *Hidden structures: a driving factor to achieve low thermal conductivity and high thermoelectric performance*, *Chem Soc Rev* 53, 6100 (2024).
7. X.-G. Wen, *Colloquium: Zoo of quantum-topological phases of matter*, *Reviews of Modern Physics* 89 (2017).
8. F. Tang, H. C. Po, A. Vishwanath, and X. Wan, *Comprehensive search for topological materials using symmetry indicators*, *Nature* 566, 486 (2019).
9. L. Landau, *The theory of phase transitions*, *Nature* 138, 840 (1936).
10. X. Chen, Y. Liu, P. Liu, Y. Yu, J. Ren, J. Li, A. Zhang, and Q. Liu, *Unconventional magnons in collinear magnets dictated by spin space groups*, *Nature* 640, 349 (2025).
11. S. A. J. Kimber *et al.*, *Dynamic crystallography reveals spontaneous anisotropy in cubic GeTe*, *Nat Mater* 22, 311 (2023).
12. K. Kim *et al.*, *Origin of the chiral charge density wave in transition-metal dichalcogenide*, *Nature Physics* 20 (2024).
13. E. S. Bozin, C. D. Malliakas, P. Souvatzis, T. Proffen, N. A. Spaldin, M. G. Kanatzidis, and S. J. L. Billinge, *Entropically Stabilized Local Dipole Formation in Lead Chalcogenides*, *Science* 330, 1660 (2010).
14. G. J. Snyder, M. Christensen, E. Nishibori, T. Caillat, and B. B. Iversen, *Disordered zinc in ZnSb with phonon-glass and electron-crystal thermoelectric properties*, *Nature Materials* 3, 458 (2004).
15. H. Pirie *et al.*, *Visualizing the atomic-scale origin of metallic behavior in Kondo insulators*, *Science* 379, 1214 (2023).
16. S. H. Skjærvo, Q. N. Meier, M. Feygenson, N. A. Spaldin, S. J. L. Billinge, E. S. Bozin, and S. M. Selbach, *Unconventional Continuous Structural Disorder at the Order-Disorder Phase Transition in the Hexagonal Manganites*, *Physical Review X* 9 (2019).
17. B. Jiang, J. Neu, D. Olds, S. A. J. Kimber, K. Page, and T. Siegrist, *The curious case of the structural phase transition in SnSe insights from neutron total*

- scattering, *Nature Communications* 14 (2023).
18. S. Mukhopadhyay, D. S. Parker, B. C. Sales, A. A. Puretzy, M. A. McGuire, and L. Lindsay, *Two-channel model for ultralow thermal conductivity of crystalline TlVSe*, *Science* 360, 1455 (2018).
 19. P. Rivera *et al.*, *Intrinsic donor-bound excitons in ultraclean monolayer semiconductors*, *Nature Communications* 12 (2021).
 20. A. Ripin, R. M. Peng, X. W. Zhang, S. Chakravarthi, M. H. He, X. D. Xu, K. M. Fu, T. Cao, and M. Li, *Tunable phononic coupling in excitonic quantum emitters*, *Nature Nanotechnology* 18, 1020 (2023).
 21. Z. H. Dong *et al.*, *Visualization of oxygen vacancies and self-doped ligand holes in LaNiO*, *Nature* 630, 847 (2024).
 22. N. Nagaosa, J. Sinova, S. Onoda, A. H. MacDonald, and N. P. Ong, *Anomalous Hall effect*, *Reviews of Modern Physics* 82, 1539 (2010).
 23. Y. Tokura, *Critical features of colossal magnetoresistive manganites*, *Reports on Progress in Physics* 69, 797 (2006).
 24. A. A. Patel, H. Y. Guo, I. Esterlis, and S. Sachdev, *Universal theory of strange metals from spatially random interactions*, *Science* 381, 790 (2023).
 25. L. D. Ye *et al.*, *Hopping frustration-induced flat band and strange metallicity in a kagome metal*, *Nature Physics* 20 (2024).
 26. L. R. Andrey Gromov, *<Fracton Matter.pdf>*, *Rev. Mod. Phys.* 96 (2024).
 27. E. Dagotto, *Complexity in strongly correlated electronic systems*, *Science* 309, 257 (2005).
 28. J. Kim *et al.*, *Coupled polarization and nanodomain evolution underpins large electromechanical responses in relaxors*, *Nature Physics* 18, 1502 (2022).
 29. H. J. Lee, M. Lee, K. Lee, J. Jo, H. Yang, Y. Kim, S. C. Chae, U. Waghmare, and J. H. Lee, *Scale-free ferroelectricity induced by flat phonon bands in HfO(2)*, *Science* 369, 1343 (2020).
 30. A. Ripin, R. Peng, X. Zhang, S. Chakravarthi, M. He, X. Xu, K. M. Fu, T. Cao, and M. Li, *Tunable phononic coupling in excitonic quantum emitters*, *Nat Nanotechnol* 18, 1020 (2023).
 31. T. T. Tran, K. Bray, M. J. Ford, M. Toth, and I. Aharonovich, *Quantum emission from hexagonal boron nitride monolayers*, *Nat Nanotechnol* 11, 37 (2016).
 32. A. A. Patel, H. Guo, I. Esterlis, and S. Sachdev, *Universal theory of strange metals from spatially random interactions*, *Science* 381, 790 (2023).
 33. D. A. Abanin, E. Altman, I. Bloch, and M. Serbyn, *Colloquium: Many-body localization, thermalization, and entanglement*, *Reviews of Modern Physics* 91 (2019).
 34. Y. Guo, S. Dhar, A. Yang, Z. Chen, H. Yao, M. Horvath, L. Ying, M. Landini, and H. C. Nagerl, *Observation of many-body dynamical localization*, *Science* 389, 716 (2025).
 35. S. J. Billinge and I. Levin, *The problem with determining atomic structure at the nanoscale*, *Science* 316, 561 (2007).
 36. R. Osborn, D. Pelc, M. J. Krogstad, S. Rosenkranz, and M. Greven, *Diffuse scattering from correlated electron systems*, *Science Advances* 11, eadt7770

- (2025).
37. A. V. Kolobov, P. Fons, A. I. Frenkel, A. L. Ankudinov, J. Tominaga, and T. Uruga, *Understanding the phase-change mechanism of rewritable optical media*, Nature Materials 3, 703 (2004).
 38. K. X. Nguyen, Y. Jiang, C. H. Lee, P. Kharel, Y. Zhang, A. M. van der Zande, and P. Y. Huang, *Achieving sub-0.5-angstrom-resolution ptychography in an uncorrected electron microscope*, Science 383, 865 (2024).
 39. J. Miao, P. Ercius, and S. J. L. Billinge, *Atomic electron tomography: 3D structures without crystals*, Science 353 (2016).
 40. K. Mallayya, J. Straquadine, M. J. Krogstad, M. D. Bachmann, A. G. Singh, R. Osborn, S. Rosenkranz, I. R. Fisher, and E. A. Kim, *Bragg glass signatures in PdErTe with X-ray diffraction temperature clustering*, Nature Physics 20 (2024).
 41. I. Mosquera-Lois, S. R. Kavanagh, A. Walsh, and D. O. Scanlon, *Identifying the ground state structures of point defects in solids*, npj Computational Materials 9 (2023).
 42. M. Zacharias, G. Volonakis, F. Giustino, and J. Even, *Anharmonic electron-phonon coupling in ultrasoft and locally disordered perovskites (vol 9, 153, 2023)*, npj Computational Materials 9 (2023).
 43. E. Cohen, H. Larocque, F. Bouchard, F. Nejdassattari, Y. Gefen, and E. Karimi, *Geometric phase from Aharonov–Bohm to Pancharatnam–Berry and beyond*, Nature Reviews Physics 1, 437 (2019).
 44. Y. Qi, N. Chen, T. Vasileiadis, D. Zahn, H. Seiler, X. Li, and R. Ernstorfer, *Photoinduced Ultrafast Transition of the Local Correlated Structure in Chalcogenide Phase-Change Materials*, Phys Rev Lett 129, 135701 (2022).
 45. Y. Qi, M. Guan, D. Zahn, T. Vasileiadis, H. Seiler, Y. W. Windsor, H. Zhao, S. Meng, and R. Ernstorfer, *Traversing Double-Well Potential Energy Surfaces: Photoinduced Concurrent Intralayer and Interlayer Structural Transitions in XTe₂ (X = Mo, W)*, ACS Nano 16, 11124 (2022).
 46. A. L. Zong *et al.*, *Spin-mediated shear oscillators in a van der Waals antiferromagnet*, Nature 620, 988 (2023).
 47. L. Xie, J. H. Feng, R. Li, and J. Q. He, *First-Principles Study of Anharmonic Lattice Dynamics in Low Thermal Conductivity AgCrSe₂: Evidence for a Large Resonant Four-Phonon Scattering*, Phys Rev Lett 125, 245901 (2020).
 48. J. G. Checkelsky, B. A. Bernevig, P. Coleman, Q. Si, and S. Paschen, *Flat bands, strange metals and the Kondo effect*, Nature Reviews Materials 9, 509 (2024).
 49. K. S. Rana, A. Singh, A. Bhui, K. Biswas, and A. Soni, *Anharmonic Phonon Vibrations of Ag and Cu for Poor Lattice Thermal Conductivity in Superionic AgCrSe and CuCrSe*, Acs Applied Energy Materials 7, 5621 (2024).
 50. L. Wang, D. Xu, S. Zhang, Y. Nie, H. Tong, and N. Xu, *Low-frequency non-phononic vibrations of amorphous solids*, Rep Prog Phys 88 (2025).
 51. Y. C. Hu and H. Tanaka, *Origin of the boson peak in amorphous solids*, Nature Physics 18, 669 (2022).
 52. *<Harmonic Vibrational Excitations in Disordered Solids and the “Boson Peak”.pdf>*.

53. J. Ding *et al.*, *Atomic dynamics in MCrX₂(M=Ag,Cu;X=S,Se) across magnetic and superionic transitions*, *Physical Review Materials* 9 (2025).
54. Q. Ren *et al.*, *Extreme phonon anharmonicity underpins superionic diffusion and ultralow thermal conductivity in argyrodite Ag(8)SnSe(6)*, *Nat Mater* 22, 999 (2023).
55. N. D. Andriushin *et al.*, *Observation of the spiral spin liquid in a triangular-lattice material*, *Nature Communications* 16 (2025).
56. S. J. Kim *et al.*, *Observation of the Anomalous Hall Effect in a Layered Polar Semiconductor*, *Advanced Science* 11 (2024).
57. C. Broholm, R. J. Cava, S. A. Kivelson, D. G. Nocera, M. R. Norman, and T. Senthil, *Quantum spin liquids*, *Science* 367 (2020).
58. H. Yan and J. Reuther, *Low-energy structure of spiral spin liquids*, *Physical Review Research* 4 (2022).
59. B. Li *et al.*, *Liquid-like thermal conduction in intercalated layered crystalline solids*, *Nat Mater* 17, 226 (2018).
60. F. F. Qi *et al.*, *Breaking 50 Femtosecond Resolution Barrier in MeV Ultrafast Electron Diffraction with a Double Bend Achromat Compressor*, *Physical Review Letters* 124 (2020).
61. H. Park *et al.*, *Observation of fractionally quantized anomalous Hall effect*, *Nature* 622, 74 (2023).
62. Y. Zeng *et al.*, *Thermodynamic evidence of fractional Chern insulator in moire MoTe(2)*, *Nature* 622, 69 (2023).
63. J. Qi *et al.*, *Magnetic evolution induced by freezing of Ag fluctuations in an intercalated transition metal dichalcogenide*, *Physical Review Materials* 9 (2025).
64. D. Sarkar, A. Bhui, I. Maria, M. Dutta, and K. Biswas, *Hidden structures: a driving factor to achieve low thermal conductivity and high thermoelectric performance*, *Chemical Society Reviews* 53 (2024).
65. B. Guzelturk *et al.*, *Dynamic lattice distortions driven by surface trapping in semiconductor nanocrystals*, *Nat Commun* 12, 1860 (2021).
66. A. Kogar *et al.*, *Light-induced charge density wave in LaTe₃*, *Nature Physics* 16, 159 (2020).